


RESEARCH

Open Access



Melanoma antigens in pediatric medulloblastoma contribute to tumor heterogeneity and species-specificity of group 3 tumors

Rebecca R. J. Collins^{1†}, Rebecca R. Florke Gee^{2,3,4,5†}, Sima Tozandehjani^{2,3}, Tara Bayat^{2,3}, Maria Camila Hoyos Sanchez^{2,3}, Juan Sebastian Solano Gutierrez^{2,3}, Barbara Breznik^{2,3,6}, Anna K. Lee^{1,5,7}, Samuel T. Peters^{5,8}, Jon P. Connelly^{5,8}, Shondra M. Pruett-Miller^{5,8}, Martine F. Roussel⁹, Dinesh Rakheja^{1,10}, Heather S. Tillman¹¹, Patrick Ryan Potts^{5,7,12*} and Klementina Fon Tacer^{2,3,5,7*} 

Abstract

Medulloblastoma (MB) is the most malignant childhood brain cancer. Group 3 MB (G3 MB) subtype accounts for about 25% of MB and is associated with the worst outcomes. Herein, we report that more than half of G3 MB tumors express melanoma antigens (MAGEs), which are potential prognostic and therapeutic markers. MAGEs are cancer-testis antigens, aberrantly expressed in several adult cancers, and associated with poorer prognosis and therapy resistance; however, their role in pediatric cancers is mostly unknown. This study aimed to determine whether *MAGEs* are activated and important in pediatric MB. We obtained formalin-fixed paraffin-embedded tumor samples of 34 patients, collected between 2008 and 2015 at the Children's Medical Center in Dallas and applied our validated reverse transcription quantitative PCR (RT-qPCR) assay to measure the expression of 23 *MAGE* genes. To validate our data, we analyzed published datasets from pediatric MB tumors and patient-derived orthotopic xenografts, totaling 949 patients. Our RT-qPCR analysis suggested that *MAGEs* were expressed in G3/4MB. Further mining of bulk and single-cell RNA-sequencing datasets confirmed that 50–75% of G3 tumors activate several *MAGEs*. Intriguingly, single-cell data analysis showed that *MAGEs* are expressed in distinct subsets of cells in *MAGE*-positive tumors and are not activated in mouse genetic models, suggesting they contribute to the tumor heterogeneity and species-specificity of G3 MB. We then examined how *MAGE* expression affects the growth and oncogenic potential by CRISPR-Cas9- and siRNA-mediated gene depletion. Depletion of *MAGEA*s, *-B2*, and *-Cs* altered cell survival, viability, and clonogenic growth due to decreased proliferation and increased apoptosis of *MAGE*-positive MB cells. These findings suggested that targeting *MAGEs* could represent a viable therapeutic strategy for G3 MB. A deeper understanding of *MAGE* regulation and function is warranted and could aid in improving prognostic and therapeutic approaches for this poorly characterized subgroup of pediatric brain tumors.

[†]Rebecca R. J. Collins and Rebecca R. Florke Gee have contributed equally to this work.

*Correspondence:
Patrick Ryan Potts
rpotts01@amgen.com
Klementina Fon Tacer
fontacer@ttu.edu

Full list of author information is available at the end of the article



© The Author(s) 2025. **Open Access** This article is licensed under a Creative Commons Attribution 4.0 International License, which permits use, sharing, adaptation, distribution and reproduction in any medium or format, as long as you give appropriate credit to the original author(s) and the source, provide a link to the Creative Commons licence, and indicate if changes were made. The images or other third party material in this article are included in the article's Creative Commons licence, unless indicated otherwise in a credit line to the material. If material is not included in the article's Creative Commons licence and your intended use is not permitted by statutory regulation or exceeds the permitted use, you will need to obtain permission directly from the copyright holder. To view a copy of this licence, visit <http://creativecommons.org/licenses/by/4.0/>.

Keywords Medulloblastoma, Tumor antigens, MAGE, Pediatric cancer, Cancer-testis antigens

Introduction

Medulloblastomas (MBs) are heterogeneous embryonal malignant tumors of the cerebellum that constitute one of the most common pediatric brain tumors with an incidence of six children per million under nine years of age [6, 26, 34, 42, 56]. MBs are categorized into four molecular subgroups: Wingless (WNT), Sonic Hedgehog (SHH), group 3, and group 4 [34, 35]. This categorization was first based on mutation profiling and expression arrays and, more recently, by DNA methylation [56, 59] and cellular origin [21, 51]. Germline mutations in the WNT inhibitor *APC* or somatic mutations in *CTNNB1* are found in almost all WNT-MBs [39, 55]. Etiology of SHH-MBs has been attributed to genetic changes in SHH signaling, including mutations in the SHH receptor *PTCH*, SHH inhibitor *SUFU*, or SHH transducer *SMO*, *GLI1/2* amplifications, and mutations in *MYCN* and *TP53* [21, 28, 55]. Group 3 and group 4 MBs (group 3/4), which account for about 60% of MB diagnoses, are the least understood with respect to disease biology and developmental origins, as they exhibit complex and sometimes overlapping mutational spectrums, DNA methylation profiles, and expression characteristics [21, 34, 35, 40, 59]. Moreover, group 3 tumors are associated with the worst prognosis of all the subgroups and are frequently metastatic at presentation [35], calling for novel approaches for effective diagnosis, prognosis, and treatment of patients with these tumors.

Surgery, radiation, and chemotherapy have improved MB patients' prognosis in the last decades, but approximately 30% of patients remain incurable, and survivors suffer severe long-term side effects from these therapies. Distinct molecular signatures of the 4 subgroups enables a personalized therapeutic approach that is already benefiting patients [42]. However, among the four subgroups, group 3 MBs exhibit the highest incidence of high-risk characteristics and therapy resistance [59]. Over the last decade, immunotherapy has rapidly changed the therapeutic landscape and prognosis for many adult cancers and is also in development for pediatric solid tumors [7]. Immunotherapies for MB have begun to undergo clinical testing (ClinicalTrials.gov: NCT03173950, NCT01326104); thus, identification of selective targets, biomarkers of responsiveness, and strategies for overcoming resistance in these tumors will be of utmost importance.

Although several brain tumor-specific targets have been identified, only a limited number of studies have investigated antigen expression and validity in pediatric populations [20]. To prevent toxicities, the best targets

for immunotherapy are tumor-associated antigens that are exclusively expressed in tumor cells with minimal expression in normal tissues [1]. Tumor-associated antigens are commonly neo-antigens generated by tumor cells because of genomic mutations [61]. Given that the somatic mutation burden increases with patient age, childhood cancers have a lower mutation burden and mutation-derived neo-antigen levels [2]. Intriguingly, tumors also commonly activate the expression of genes normally restricted to male germ cells, referred to as cancer-testis antigens (CTAs), as expression outside of their naturally immune-privileged site in the testis can activate an immune response [17]. Melanoma-associated antigens (MAGEs) were the first CTAs discovered [14, 32, 58]. The *MAGE* family encompasses approximately 40 conserved genes divided into two major subgroups: Type I and Type II [14]. While Type II *MAGEs* are ubiquitously expressed and implicated in neurodevelopment, Type I *MAGEs* are CTAs with normal expression in the testis but aberrantly expressed in various cancers [14, 15, 45, 58]. Furthermore, Type I *MAGEs* predict poor patient prognosis and are remarkable candidates for immunotherapy targets [3, 14, 15, 32, 45, 58]. *MAGEs* are heavily investigated in immunotherapy of adult cancers [3], but very little is known about their expression and role in pediatric tumors [27, 50].

In this study, we performed the first comprehensive analysis of all Type I *MAGE* CTAs (*MAGEA*, *-B*, and *-C* subfamily members) in pediatric MBs and found that several are expressed in more than 60% of group 3 MBs and are required for the viability and growth of cells in which they are expressed. Collectively, these data provide novel insights into the antigen landscape of pediatric MBs and show that more than half of group 3 tumors activate *MAGE* genes, presenting potential stratifying and therapeutic options.

Materials and methods

Materials

Refer to Extended Materials and Methods.

Medulloblastoma patient samples

With appropriate institutional review board approval, we searched for brain tumor pathology cases diagnosed as medulloblastoma with a histologic subtype during the years 2008–2015 that also had FFPE tissue archived at Children's Medical Center Dallas. Paraffin blocks and glass slides were examined to confirm the diagnosis and ensure adequate tissue availability. 34 de-identified cases were selected, and all except MT23 had sufficient material for complete analysis. Scrolls 10 mm thick were obtained from at least one block of tissue for each case. Genetic subgroup classification of the medulloblastoma

cases was done using paired expression of DKK1 (Bio-Rad, qHsaCED0043208) and WIF1 (Bio-Rad, qHsaCID0006122) or SFRP (Bio-Rad, qHsaCID0015548) and HHIP (Bio-Rad, qHsaCID0018207), where >0.01 value of both DKK1 and WIF1 corresponded to WNT subgroup or >0.01 value of both SFRP and HHIP corresponded to SHH subgroup; all other cases were classified as Group 3/4 subgroup. MB subgroup was confirmed by immunohistochemistry staining profile in 8 cases (Table S1). No cases had an immunoprofile that refuted the genetic subgroup (one case was unable to be classified by immunostains).

Ethics approval and consent to participate

The present study was performed in accordance with the guidelines proposed in the Declaration of Helsinki and with institutional approval. FFPE tissue collection and phenotypic and tissue analyses were conducted under UT Southwestern Institutional Review Board approval IRB STU 102015-047. MT17 cells were cultured with patient/family consent under Pediatric Biospecimen Repository protocol IRB STU 082010-115. MFR research was conducted under IRB NBTP01-UT-XPB. All animal studies were approved by the Animal Care and Use Committee and performed in accordance with best practices outlined by the NIH Office of Laboratory Animal Welfare.

Cell culture

DAOY (Cat. No. HTB-186) and D283 (Cat. No. HTB-185) cells were purchased from American Type Culture Collection (ATCC) and grown in DMEM supplemented with 10% FBS, 2 mM L-glutamine, and $1\times$ antibiotic–antimycotic (100 units/mL penicillin, 100 mg/mL streptomycin, and 0.25 mg/mL Amphotericin B). At the time of patient surgery, MT17 tumor cells were obtained from the Pediatric Biospecimen Repository; these cells were collected as residual tissue from the patient's surgical resection specimen, cultured in minimum essential media (MEM) supplemented with 10% FBS and 10% BM-Condensed (Roche) at the affiliated hospital, and then cryogenically stored. We subsequently cultured MT17 cells in DMEM supplemented with 10% FBS, 2 mM L-glutamine, $1\times$ antibiotic–antimycotic, and 10% BM-Condensed. D425 cells, generously provided by Dr. Darell Bigner of Duke University [16], were grown in ultra-low attachment flasks with NeuroCult NS-A Basal Medium (Human) (STEMCELL Technologies) with NeuroCult NS-A Supplement (STEMCELL Technologies), $1\times$ N-2 Supplement (Thermo Fisher), $1\times$ B-27 Supplement minus vitamin A (Thermo Fisher), $1\times$ penicillin/streptomycin, $1\times$ GlutaMAX (Thermo Fisher), 0.2% (v/v) BSA (Sigma-Aldrich), and 2 μ g/mL heparin (STEMCELL

Technologies). To support optimal growth of D425 cells, 0.25 μ L of each human recombinant EGF (200 μ g/mL) and human bFGF (200 μ g/mL) were added per mL of medium every three days. D425 cells were dissociated with AccuMax (Thermo Fisher). All cells were incubated in a humidified atmosphere at 37 °C with 5% CO₂. Cell counts were obtained with a hemocytometer or with a Countess II Automated Cell Counter using trypan blue staining.

RNA isolation and reverse transcription quantitative PCR (RT-qPCR)

RNA from FFPE tissues was isolated using the Qiagen RNeasy FFPE Kit according to the manufacturer's protocol. RNA from cell cultures, mouse tumors, and PDOX samples was isolated using the TRIzol reagent (Invitrogen) according to the manufacturer's directions. RNA was treated with DNase I (Roche) in 4.5 mM MgCl₂ to eliminate genomic DNA contamination, and cDNA was prepared from 4 μ g of DNase-treated RNA using the Applied Biosystems High-Capacity cDNA Reverse Transcription (Applied Biosystems) kit in 100 μ L final volume. Following cDNA synthesis, RNase-free water was added to increase the sample volume to 300 μ L. Gene expression levels were measured by RT-qPCR in triplicate wells of a 384-well reaction plate with 22 ng of cDNA/well on an Applied Biosystems 7900HT with SYBR Green chemistry. As previously published [15], specific primers were used for each Type I *MAGE* (150 nM concentration; Table S3). Relative gene expression was calculated by normalizing against 18S values and calibrated across different plates. Extended Materials and Methods provides additional details.

MAGE KO library

Up to five sgRNAs for each *MAGE* and *MAGE*-related gene were designed and assessed for off-target potential in silico based off homology to other sites in the genome. sgRNAs were cloned into the lentiGuide-Puro vector (Addgene #52963). The finished library consisted of 494 sgRNAs targeting 155 human and mouse genes, along with non-targeting negative controls making up 2.5% of the library (Table S2). Validation to check sgRNA presence and representation was performed using `calc_auc_v1.1.py` (<https://github.com/mhegde/>) and `count_spacers.py` [25]. Viral particles were produced by the St. Jude Vector Laboratory.

CRISPR dropout screen

The generation of DAOY-Cas9 stable expressing cells is described in Extended Materials and Methods. For the screen, 40,000 DAOY-Cas9 stable expressing cells were seeded in 10 wells of 6-well plates. The next day, cells

were transduced with the MAGE KO library (MOI < 0.5) in the presence of 8 µg/mL (final concentration) polybrene (Sigma-Aldrich). 48 h after viral transduction, 500,000 cells were collected as the Day 0 sample for NGS analysis, and the remaining cells were selected with 0.5 µg/mL puromycin. Cells were split when about 80–90% confluent, and at least 500,000 cells were collected at this time by washing with PBS, pelleting cells, and freezing cells at – 80 °C. At the end of 30 days, genomic DNA was extracted from the samples with the DNEasy Blood & Tissue Kit (Qiagen) following manufacturer's protocol. St. Jude Center for Advanced Genome Editing (CAGE) PCR amplified the integrated sgRNAs as described in the Broad GPP protocol (<https://portals.broadinstitute.org/gpp/public/resources/protocols>). The St. Jude Hartwell Center Genome Sequencing Facility provided NGS sequencing using single end 100 cycle kit on a NovaSeq 6000 (Illumina). NGS data were analyzed using MAGECK-VISPR/0.5.7 [33]. Results are reported as log₂ fold change for Day 30 sgRNA reads using the Day 0 reads as the baseline, and datapoints represent triplicate samples for all sgRNAs targeting a specific gene. The abundance of each sgRNA over time was determined by setting the Day 0 abundance as 100%.

siRNA transfection

Lipofectamine RNAiMAX (Invitrogen) was used for all transfections according to the manufacturer's instructions. DAOY and D283 cells were reverse transfected with 33.3 nM siRNA, plated in 6-well or 96-well plates with the media changed 24 h after transfection, and collected 48–72 h after transfection for qPCR or western blotting. D425 cells were plated in Opti-MEM in 6-well or 96-well plates, transfected with 200 nM siRNA, cultured in Opti-MEM for 20 h after transfection, and then grown in complete media. 90 h after transfection of D425 cells, AlamarBlue viability assay was performed, or the cells were collected for qPCR or western blotting. Control siRNAs for LonRF (oligo # 3012482021-000160, –000170) and UBB (oligo # 3030837381-000300, –000310) were purchased from Sigma. Sequences of all other siRNAs (Sigma-Aldrich) are included in Table S3.

Viability assays

For viability assays, cells were seeded 1,000–5,000 cells/well in 96-well plates and grown for 72–96 h following reverse transfection. AlamarBlue (Bio-Rad) or CellTiter-Glo Luminescent Cell Viability Assay (Promega) was used to measure cell viability, along with a BioTek Cytation 5 (Agilent) automated plate reader that measured fluorescence or luminescence, respectively. Results are reported as a percentage normalized to the averaged

siRevL1 or siLonRF control. Experiments were repeated up to three times on separate days.

BrdU immunofluorescence assay

4000 DAOY cells/well were plated in 8-well chambered glass slides (Nunc Lab-Tek II) and reverse transfected with siRNA. After 48 h, 10 µM (final concentration) of BrdU (BD Pharmingen BrdU FlowKit 559619) was incubated with cells for 4 h. Then, cells were washed with ice-cold PBS, fixed with methanol for 10 min at – 20 °C, and washed with room temperature (RT) PBS. Cells were incubated in 2 M hydrochloric acid for 20 min at RT to dissociate dsDNA, washed with PBS, and permeabilized with blocking solution [PBS containing 0.2% (v/v) Triton X-100 and 3% (w/v) bovine serum albumin (BSA)] for 20 min at 4 °C. Anti-BrdU rat antibody conjugated to FITC (ab74545; 1:250 or 1:500) was incubated with cells at RT for 1 h in the dark. After washing with PBS containing 0.2% Triton X-100, nuclei were stained with DAPI. Stained cells were then mounted with Aqua-Poly/Mount (Polysciences) and imaged at 20× with a Leica AF6000 microscope and appropriate filters. For each slide, an untreated well with and without BrdU was used to establish background fluorescence. Images were analyzed with ImageJ and BrdU-positive cells determined by counting at least 100 cells for each condition.

Clonogenic assays

DAOY cells were reverse transfected in 6-well plates and allowed to grow overnight. Cells were then trypsinized, diluted, mixed with an equal volume of warm agar (0.35% final), and 1×10^4 cells/well placed in 6-well plates over a 0.5% agar base. After cooling for 20 min, 1 mL culture media was added to the top of each well. After 24 h, individual cells were counted within 10 separate fields using an inverted microscope with a 20× objective, to ensure equal cell densities between wells. Plates were incubated for 4 weeks with media changed 1–2 times a week. DAOY colonies were imaged with a 4× objective and all colonies > 50 µm were counted in 9 separate fields. The soft agar assay with D283 cells and the colony formation assay is described in Extended Materials and Methods.

Preparation of cell lysates and western blotting

Cell lysates were prepared as previously described [31], and the total protein concentration quantified with the Micro BCA Protein Assay Kit (Thermo Scientific). Lysates were prepared in SDS sample buffer, resolved on SDS-PAGE gels, and transferred to nitrocellulose membranes. Membranes were blocked with 5% BSA in TBST [25 mM Tris pH 8.0, 2.7 mM KCl, 137 mM NaCl, 0.05%

(v/v) Tween-20] and incubated with primary antibodies. The following antibodies were used: anti-MAGEB2 [31], anti-MAGEA2 [11], anti-MAGEA3 (Abcam, ab223162), anti-Cleaved PARP (Asp214) (19F4) (Cell Signaling Technology, #9546), anti-TRIM28 (Abcam, ab22553), anti-Cas9 (Abcam, ab191468), anti-GAPDH (D16H11) (Cell Signaling Technology, #5174), and anti- β -actin (Abcam, ab6276). After three washes with TBST, membranes were incubated with secondary antibodies, washed an additional three times, and detected via chemiluminescence using ECL detection reagent (GE Healthcare, RPN2209).

MB microarray and single-cell RNA-sequencing (scRNA-seq) datasets

GlioVis data portal [5] was used to analyze and visualize Cavalli et al. [8] data of 763 MB patient samples (GSE85218). We obtained the scRNA-seq datasets of primary MB patient samples and patient-derived xenografts from GSE119926 [21] and GSE155446 [47]. Average expression of *MAGE* genes was calculated for all the cells of each patient/xenograft to generate heatmaps. Additional details are provided in Extended Materials and Methods.

Plotting and statistical analyses

Except Figures S1, S2B–F, and S3, plots were made in GraphPad Prism 10. Results are expressed as the mean \pm standard deviation from at least two independent experiments with individual data points indicated. Significance was assessed with one-way or two-way ANOVA followed by Dunnett's multiple comparisons test for all samples compared to the control [$P \leq 0.05$ (*), $P \leq 0.01$ (**), $P \leq 0.001$ (***), $P \geq 0.05$ (non-significant, ns)].

Results

Type I *MAGE* CTAs are expressed mainly in group 3 of pediatric medulloblastoma

To determine the frequency of *MAGE* expression in pediatric MB, we measured expression levels of Type I *MAGEs* in patient tumors (Fig. 1A). We obtained FFPE tissue samples from 34 patients, collected between 2008 and 2015, from the Children's Medical Center Dallas pathology archives and performed RT-qPCR. This cohort of MB samples contained one unknown, one WNT, 11 SHH, and 21 group 3/4 molecular subtypes (Table S1). To confirm the subgroups, we measured WNT inhibitors [WNT Inhibitor Factor 1 (WIF1) and Dickkopf 1 (DKK1)] and SHH-target genes (SFRP1 and HHIP) known to be produced by WNT- and SHH-MBs, respectively [41, 44]. Although type I *MAGEs* are not expressed in normal brain tissues (Figure S4F) [15], 66% of the

group 3/4-MBs expressed at least one *MAGE* gene, with many tumors expressing multiple *MAGEs* (Fig. 1B). In contrast, the WNT- and SHH-MBs were positive for only one or two *MAGEs* (except for MT29 which expressed three). Our analysis suggested disease-specific expression of Type I *MAGEs* in group 3/4 MBs, in line with their common expression in more aggressive adult tumors [14].

To validate our findings, we analyzed publicly available and published datasets for *MAGE* expression (Fig. 1A). We first examined the GlioVis database [5] for *MAGE* mRNA levels in 763 pediatric MBs analyzed by microarray [8] and found that *MAGEA1*, *-A3*, *-A11*, *-B2*, and *-C* subfamily members were detected. *MAGEA3* expression was highly enriched in group 3, and its expression was linked to worse survival (Figs. S1A and S1B). The expression of other Type I *MAGEs*, like *MAGEB2*, did not show any specific pattern (Fig. S1C), except *MAGEC3* enrichment in the WNT subgroup (Fig. S1D). We then specifically looked for RNA sequencing (RNA-seq) data, as microarray probes are often not specific enough to distinguish between several genes in the *MAGEA*, *-B*, and *-C* subfamilies that exhibit high levels of similarity [14]. Our analyses of bulk RNA-seq data from the PeCan database (St. Jude Children's Research Hospital; N=98; Fig. 1C) and scRNA-seq data published by Hovestadt et al. [21] (N=25; Fig. 1D) and Riemondy et al. [47] (N=29; Fig. S2A) revealed a similar trend in *MAGE* expression in MB tumors (Fig. 1B). By combining the single-cell expression for each tumor, we found that more than half of all the tumors analyzed by scRNA-seq were positive for >3 *MAGEs*, with group 3 MBs exhibiting the highest expression levels of multiple Type I *MAGEs* (Fig. 1D). These data support our initial finding that *MAGE* CTAs are expressed in a significant portion of patients with group 3 MBs and may represent a stratifying marker for this heterogeneous group of patients. We included the expression of marker genes along with methylation subtype classification in Fig. 1D; however, *MAGE* gene expression does not appear to be specifically associated with any particular subtype within group 3 MB.

Given that group 3 MBs are characterized by genomic amplification or overexpression of *MYC* [21], we included *MYC* expression data in our analyses (Figs. 1C and 1D). Additionally, for some of the original 34 patient tumor samples analyzed from Children's Medical Center Dallas, immunohistochemistry and molecular studies were performed at the originating or referring institutions as part of the clinical diagnostic workup, which also included assessment of *MYC*/*MYCN* expression or amplification (Table S1). These analyses supported our RT-qPCR-based

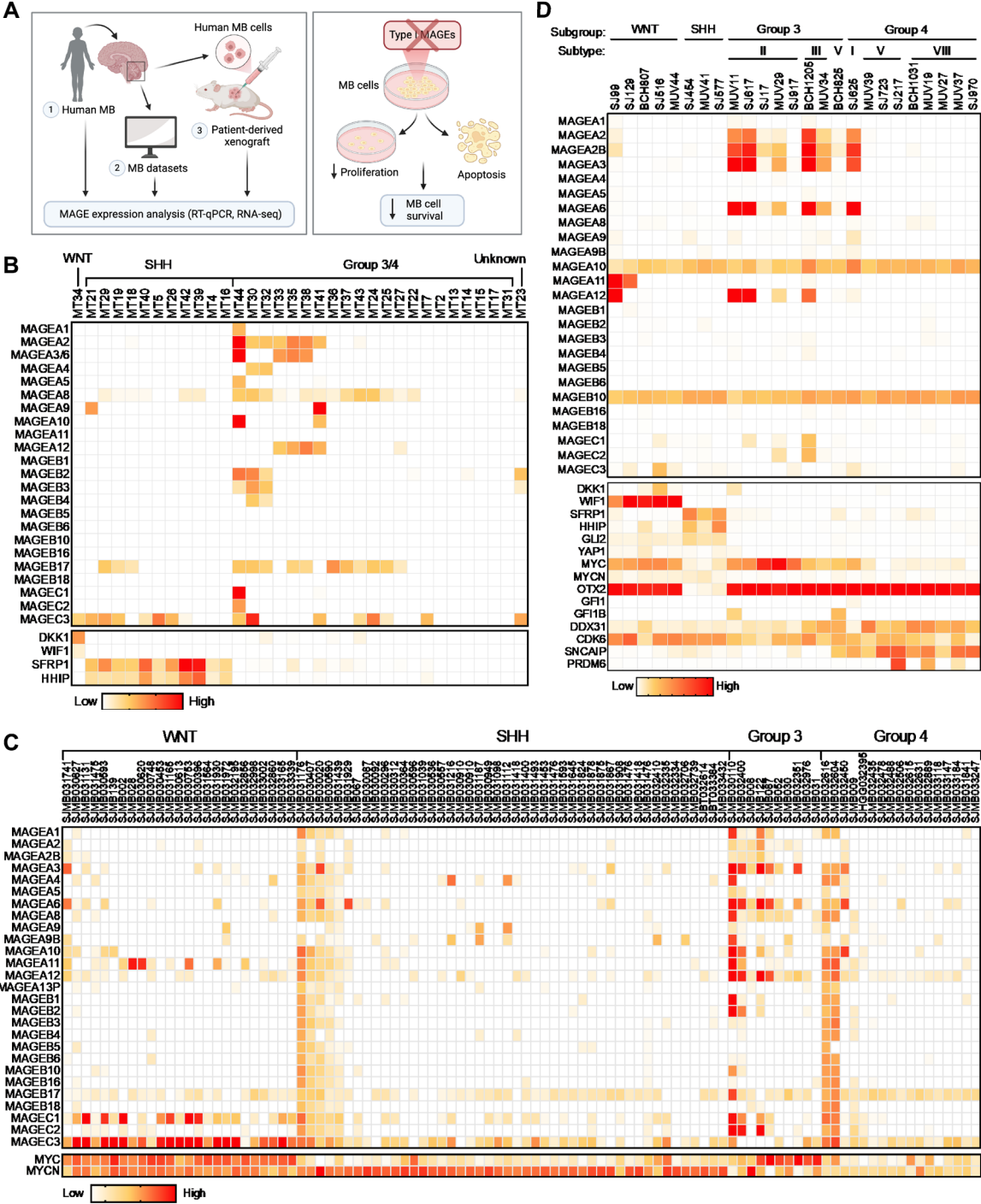


Fig. 1 Group 3 medulloblastomas express multiple Type I *MAGEs*. **A** Overview of data presented herein. Heatmaps show the expression of *MAGEs* in pediatric medulloblastomas with indicated subtypes, as determined by **B** qPCR (Pediatric Biospecimen Repository at Children's Medical Center Dallas), **C** RNA-seq (Pediatric Cancer Genome Project, data downloaded 2.4.2020), or **D** scRNA-seq (GSE119926 dataset [21]). Patient clinical details for the samples included in **B** can be found in Table S1

MB subgroup classification that was based on the expression of *DKK1* and *WIF1* or *SFRP1* and *HHIP*. Combined with more comprehensive data presented in Fig. 1C, D, these findings support that *MYC* expression is highest in group 3 MBs, though *MYC* is also notably elevated in WNT MBs. Within group 3, however, *MAGE* expression

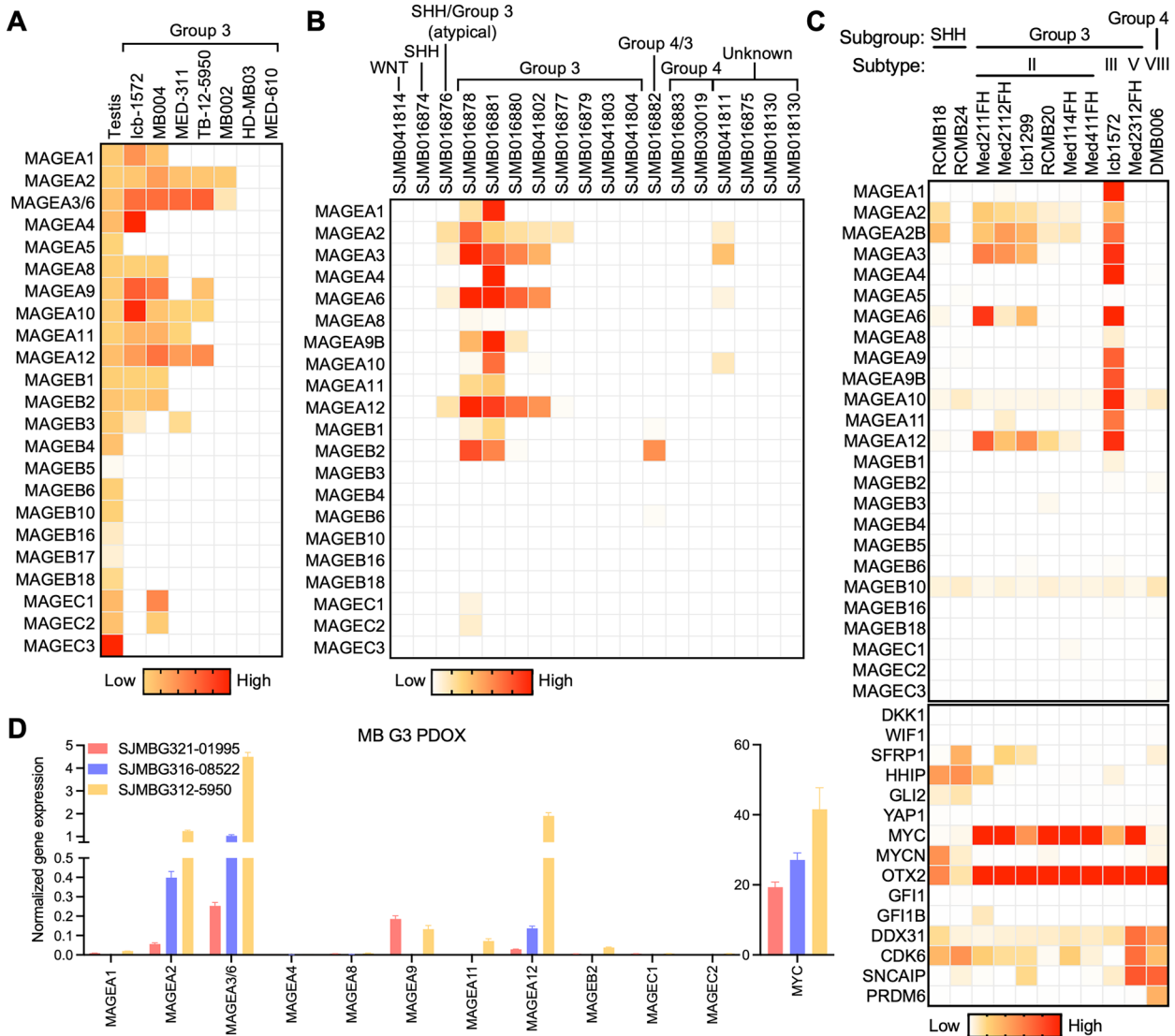


Fig. 2 Patient-derived orthotopic xenograft (PDOX) models from group 3 medulloblastomas express multiple *MAGEs*. Heatmaps show the expression of *MAGEs* in PDOX models, as determined by **A** RT-qPCR (generated in Dr. Martine Roussel lab [52]), **B** RNA-seq (generated and analyzed in Dr. Martine Roussel lab [52]), or **C** scRNA-seq (GSE119926 dataset [21]). **D** Graph shows the expression of *MAGEs* and *MYC*, as determined by RT-qPCR, in group 3 MB PDOX cells with *MYC* amplification

appears to be inversely correlated with *MYC* expression (Figs. 1C and 1D), suggesting that *MAGEs* may define a distinct subgroup of group 3 MB tumors. To further address the potential correlation between *MAGE* and *MYC* expression, Cancer Cell Line Encyclopedia (CCLE) [4] data were downloaded from the DepMap portal to calculate correlation values between expression levels for each *MAGE* and *MYC* in medulloblastoma cell lines (Fig. S1E). Based on these correlation values for *MYC* and each *MAGE* (e.g., *MAGEA2*: 0.22, *MAGEA8*: 0.24, *MAGEA10*: 0.33, *MAGEB17*: 0.35, and *MAGEB16*: -0.45), there

does not appear to be a clear pattern of *MYC*-dependent *MAGE* expression in group 3 tumors.

Patient-derived orthotopic xenograft (PDOX) models recapitulate tumor *MAGE* expression signature

We then analyzed the expression of *MAGE* genes in patient-derived orthotopic xenograft (PDOX) models generated from pediatric brain tumor patients treated at St. Jude Children's Research Hospital (Fig. 1A) [52]. RT-qPCR and RNA-seq analyses revealed that these PDOX models at least partially recapitulated the patterns of *MAGE* expression seen in patients (Figs. 1 and

2). In particular, the majority of group 3 PDOX models expressed multiple Type I *MAGEs* (Fig. 2). Our analysis of a published PDOX scRNA-seq dataset [21] showed that 66% of the samples express at least one *MAGE*, and group 3 PDOX models are positive for multiple *MAGEs* (Fig. 2C). These findings demonstrate that several Type I *MAGEs* are also expressed in PDOX models derived from group 3 MBs.

***MAGEs* are expressed in distinct subsets of cells in *MAGE*-positive group 3 MB tumors**

To determine the heterogeneity of *MAGE* expression in each tumor, we analyzed *MAGE* expression in MB tumors on a single-cell level. In the dataset published by Riemondy et al. [47], most malignant cells were grouped according to different individuals, while myeloid cells, lymphocytes, and oligodendrocytes were not separated between patients (Fig. S2B), alluding to interindividual differences in MB tumors. In line with the ubiquitous expression pattern reported for most Type II *MAGEs* (Fig. S4F) [15], these genes are expressed in all cell types without showing a specific pattern, as shown for *MAGED2* expression distribution between neoplastic and non-neoplastic cells (Fig. S2C). However, expression of Type I *MAGEs* (i.e., *MAGEA3*, *-A10*, and *-A12*) was restricted to malignant cells from group 3 MBs and to specific patients (Figs. S2D–F). For example, patient 1130 expressed *MAGEA3*, *-A6*, and *-A12*, with some cells from patients 1355 and 1028 also expressing *MAGEA3* and *-A6* (Figs. S2D, S2F, and S3C). On the other hand, the expression of *MAGEA10* was restricted to patient 1167 (Fig. S2E). All these samples had representation of different subpopulations of neoplastic cells (mitotic, undifferentiated progenitor, and neuronally differentiated); however, the expression of *MAGEs* was not restricted to specific subpopulations.

From the scRNA-seq dataset published by Hovestadt et al. [21], we determined the percentage of cells from the *MAGE*-positive group 3 MBs expressing each Type I *MAGE* (Table S4) and the number of Type I *MAGEs* expressed (Table S5). We found that *MAGEA2/2B*, *-A3*, *-A6*, *-A10*, *-A12*, and *-B10* were expressed in at least 20% of cells in three or more group 3 MB samples (Table S4). In all but one group 3 MB sample, the majority of cells expressed one or two *MAGEs* (Table S5).

Further, we wanted to know whether these *MAGEs* are activated in the same cells or distinct cell groups. Our clustering visualization of all *MAGE*-expressing cells from all the patients suggested that different *MAGE* genes are often expressed in different subsets of cells (Figs. S3A and S3B) [21, 47]. This pattern is also apparent when zoomed in on individual patients (Fig. S3C) [47] and as also seen for *MAGEA3* and *-A10* in Figs. S2D and

S2E. Given that the functions of individual *MAGE* proteins may be discrete, this mosaic *MAGE* expression may contribute to tumor heterogeneity.

***MAGE* expression contributes to the species-specificity signature of group 3 MBs**

To understand tumor initiation and identify tumor-specific therapeutic targets, previous studies have focused on identifying the cellular origins of childhood MB [21, 48, 57]. Comparison of human cerebellar tumors with the developing murine cerebellum indicated that WNT, SHH, and group 3 tumors consisted of subgroup-specific undifferentiated and differentiated neuronal-like malignant populations, whereas group 4 tumors were exclusively comprised of differentiated neuronal-like neoplastic cells [21, 57]. The tumor cells expressing *MAGEs* likely comprise undifferentiated progenitor-like cells with high MYC activity (subpopulation program B), as Hovestadt et al. [21] reported that more than 88% of the cells from the group 3 MBs, in which multiple *MAGEs* were expressed (Figs. 1D, 2C, and S3A), were annotated as program B.

The lack of high-confidence correlations between murine cerebellar populations and group 3 MBs [21, 57] suggests a cell of origin for group 3 MB that is absent in the developing murine cerebellum. Although the mouse cerebellum shares many features of lamination, circuitry, neuronal morphology, and foliation with humans, the human cerebellum has 750-fold greater surface area, increased neuronal numbers, altered neuronal subtype ratios, and increased folial complexity, suggesting species-specific neuronal progenitors [19]. Indeed, Smith et al. [51] recently reported that group 3 MBs are closely aligned with human fetal rhombic lip progenitors. Intriguingly, we could not detect expression of any Type I *Mages* in tumors from diverse MB mouse models [i.e., cMyc overexpression (*Myc* OE), *Myc* overexpression with co-deletion of *p53* and *p18* (*Trp53*^{-/-}, *Cdn2c*^{-/-}, MYCN), co-deletion of *Ptch* and *p53* (*Ptch1*[±], *Trp53*^{-/-})] (Table S6) [49]. These data suggest that Type I *MAGE* genes have species-specific oncogenic potential and expression regulation, which is in line with the recent evolution and expansion of Type I *MAGE* genes, often-times in a species-specific manner [14, 15].

Disrupted expression of *MAGEs* decreases the viability of medulloblastoma cells

To determine whether *MAGEs* contribute to MB cell viability, as reported in other cancer cell types [9, 45, 60, 62], we evaluated *MAGE* expression profiles in MB cell lines (Fig. 3A), many of which express multiple Type I *MAGEs* like the MB tumor and PDOX samples (Figs. 1 and 2). DAOY and D283 MB cell lines were selected for

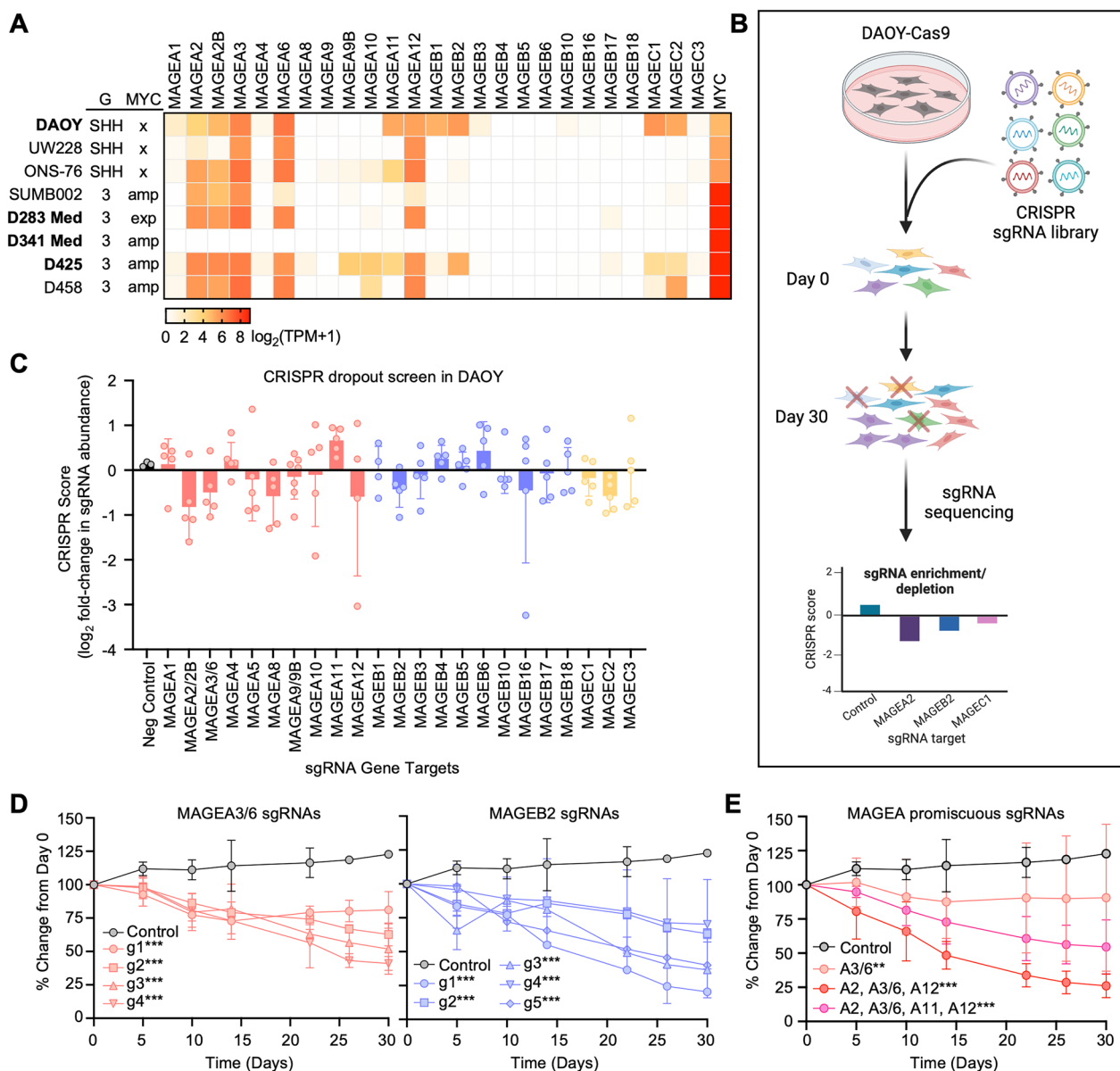


Fig. 3 Depleted *MAGE* expression decreases the viability of DAOY medulloblastoma cells. **A** Expression of Type I *MAGE*s in medulloblastoma cell lines (data downloaded from DepMap, version 23Q2, on October 11, 2023). The MB subgroup (G) classification and MYC status (amp—amplification; exp—overexpression) are indicated [22]. Values are inferred from RNA-seq data using the RSEM tool and are reported after \log_2 transformation, using a pseudo-count of 1; $\log_2(\text{TPM} + 1)$. **B** Experimental schematic of CRISPR dropout screen performed in DAOY-Cas9 stable expressing cells. **C** CRISPR score (\log_2 fold change from day 0) was calculated for the abundance of all sgRNAs on day 30. Data points show the average CRISPR score of each sgRNA targeting a particular Type I *MAGE* ($n = 3$). **D** Percent change is shown over time for each sgRNA targeting *MAGEA3/6* (left) or *MAGEB2* (right). Data points show the average percent change for each sgRNA from triplicate samples. **E** Promiscuous sgRNAs targeting multiple *MAGE*s were depleted over time. Data points show the average percent change from day 0 for all sgRNAs targeting the same group of multiple *MAGEA* genes ($n = 3$). Significance was assessed with two-way ANOVA followed by Dunnett's multiple comparisons test for samples compared to the non-targeting control sgRNAs [$P \leq 0.01$ (*), $P \leq 0.001$ (***)]

experiments after confirming their patterns of *MAGE* expression (Figs. 3A, S4A, and S4G). First, we generated DAOY-Cas9 stable expressing cells and confirmed Cas9 activity (Figs. S4B and S4C). Then, we conducted a CRISPR dropout screen in DAOY-Cas9 cells transduced

with a lentiviral pooled library containing non-targeting sgRNAs (negative controls) and approximately five sgRNAs targeting each *MAGE* gene (Fig. 3B). Many of the sgRNAs targeting the ubiquitously expressed Type II *MAGE*s (Figs. S4F and S4G), particularly *NSMCE3*

(*MAGEG1*) and *MAGEL2*, were depleted by day 30 (Figs. S4D and S4E), which supports previous reports on their importance for cell viability [14, 46, 54]. In addition, many of the sgRNAs targeting the Type I *MAGE* CTAs (Fig. S4F) yielded negative CRISPR scores, including *MAGEA3/6* and *-B2* (Figs. 3C and 3D). Besides specific sgRNAs that only targeted one *MAGE* gene, the pooled library also contained promiscuous sgRNAs that targeted multiple *MAGEs* with similar sequences. Interestingly, the 14 sgRNAs targeting *MAGEA* subfamily members were depleted over time, with many showing reductions similar to or lower than that of the specific *MAGEA3/6* sgRNAs (Fig. 3E).

As another approach to determine which *MAGE* proteins contribute to cell viability, we transiently knocked down Type I *MAGEs* in DAOY and D283 MB cells using siRNAs. The siRNA-mediated knockdown of Type I *MAGEs* decreased MB cell viability (Figs. 4A, B, and S5A). We confirmed the reduced expression of siRNA targets by RT-qPCR (Fig. S4H), with siPanMAGEA2 and *-A4* affecting the predicted *MAGEAs* (Fig. S4I). Interestingly, DAOY cell viability was reduced the most upon knockdown of *MAGEB2* (Figs. 4A and S6B). Cell viability was minimally affected by knocking down *MAGEs* in MT17 MB cells, which do not express Type I *MAGEs*, suggesting that the effect on cell viability in DAOY cells was dependent on *MAGE* expression (Figs. 1A and 4C).

We repeated the studies using two additional MB cell lines, recognizing that DAOY and D283 may not be ideal models for group 3 (Fig. 3A). *MYC* expression is upregulated in group 3 MB cell lines due to either overexpression (D283) or amplification (D425 and D341), leading to similar *MYC* expression levels regardless of the underlying mechanism (Figs. 3A and S5A). D425 is of particular interest because it expresses *MAGEs* at high levels, whereas *MAGE* expression in D341 cells is negligible (Figs. 3A and S5A). In line with our findings in DAOY and MT17 MB cells, knockdown of *MAGEs* decreased viability in D425 but not D341

MYC-amplified MB cell lines (Figs. 4D, 4E, and S5B–D). These results confirm that the negative effect on MB cell viability is dependent on *MAGE* expression and possibly independent of *MYC* expression.

MAGEs contribute to medulloblastoma cell proliferation and growth

The decreased cell viability observed upon depletion of *MAGEA* and *MAGEB2* proteins (Figs. 3C–E, 4A, 4B, and S6B) suggested that *MAGEs* may play a role in cell proliferation. Indeed, siRNA-mediated knockdown of *MAGEAs* and *MAGEB2* moderately decreased the percentage of BrdU-positive cells, particularly in cells transfected with siPanMAGEA4, which knocked down all *MAGEAs* (Fig. 5A, B). Next, we evaluated whether Type I *MAGEs* participate in anchorage-independent growth as a marker of malignancy. The number of colonies formed in soft agar by DAOY cells transfected with *MAGEA* or *-B2* siRNAs was significantly reduced compared to control cells (Figs. 5C, 5D, S6C, and S6D), indicating that these *MAGEs* contribute to tumorigenicity. The siRNA-mediated depletion of *MAGEAs* and *-B2* in D283 cells also led to decreased colony formation (Figs. S6E and S6F). These reductions in cell proliferation and colony growth upon *MAGE* knockdown may be due to increased cell death by apoptosis or necrosis, at least for *MAGEB2* knockdown, which led to the production of cleaved PARP (Fig. 5E) and a higher percentage of propidium iodide (PI)-positive cells (Figs. S6G and S6F). Together, these data suggest that expression of Type I *MAGEs* in MB cancer cells leads to dependence on their function(s), and *MAGE* depletion decreases cell viability or even leads to cell death.

Discussion

The tumor antigen landscape of pediatric MB remains largely unexplored. This report is the first comprehensive analysis of the expression of all Type I *MAGEs* in pediatric MBs and their association with MB subgroup, as earlier studies did not report MB subtype or were classified

(See figure on next page.)

Fig. 4 Knockdown of *MAGEs* decreases the viability of medulloblastoma cells. **A** DAOY or **B** D283 medulloblastoma cells were transfected with the indicated siRNA(s), and AlamarBlue or CellTiter-Glo viability assay, respectively, was performed after 3 days. The viability percentage was calculated by normalizing to the siRevL1 control. Graphs show normalized data points for at least 4 replicates from 2–6 experiments. **C** Compared to MT17 cells, the siRNA-mediated knockdown of the indicated *MAGEs* significantly reduces DAOY cell viability, as determined by two-way ANOVA. Relevant DAOY data was extracted from **A** for comparison with MT17, as the experiments could not be done at the same time. Heatmap shows expression of selected Type I *MAGEs*, as determined by RT-qPCR, in DAOY and MT17 cells. **D** AlamarBlue viability assay was performed 90 h after transfecting D425 cells, and the graph shows the viability percentage normalized to siLONRF control. Significance for viability data was assessed with one-way ANOVA followed by Dunnett's multiple comparisons test for samples compared to the control [$P \leq 0.05$ (*), $P \leq 0.01$ (**), $P \leq 0.001$ (***), $P > 0.05$ (non-significant, ns)]. **E** D425 cells were harvested for western blot analysis 90 h after siRNA transfection. The *MAGEA2* antibody used in the top blot does not discriminate among the *MAGEA* proteins, due to their similarity in size and sequence

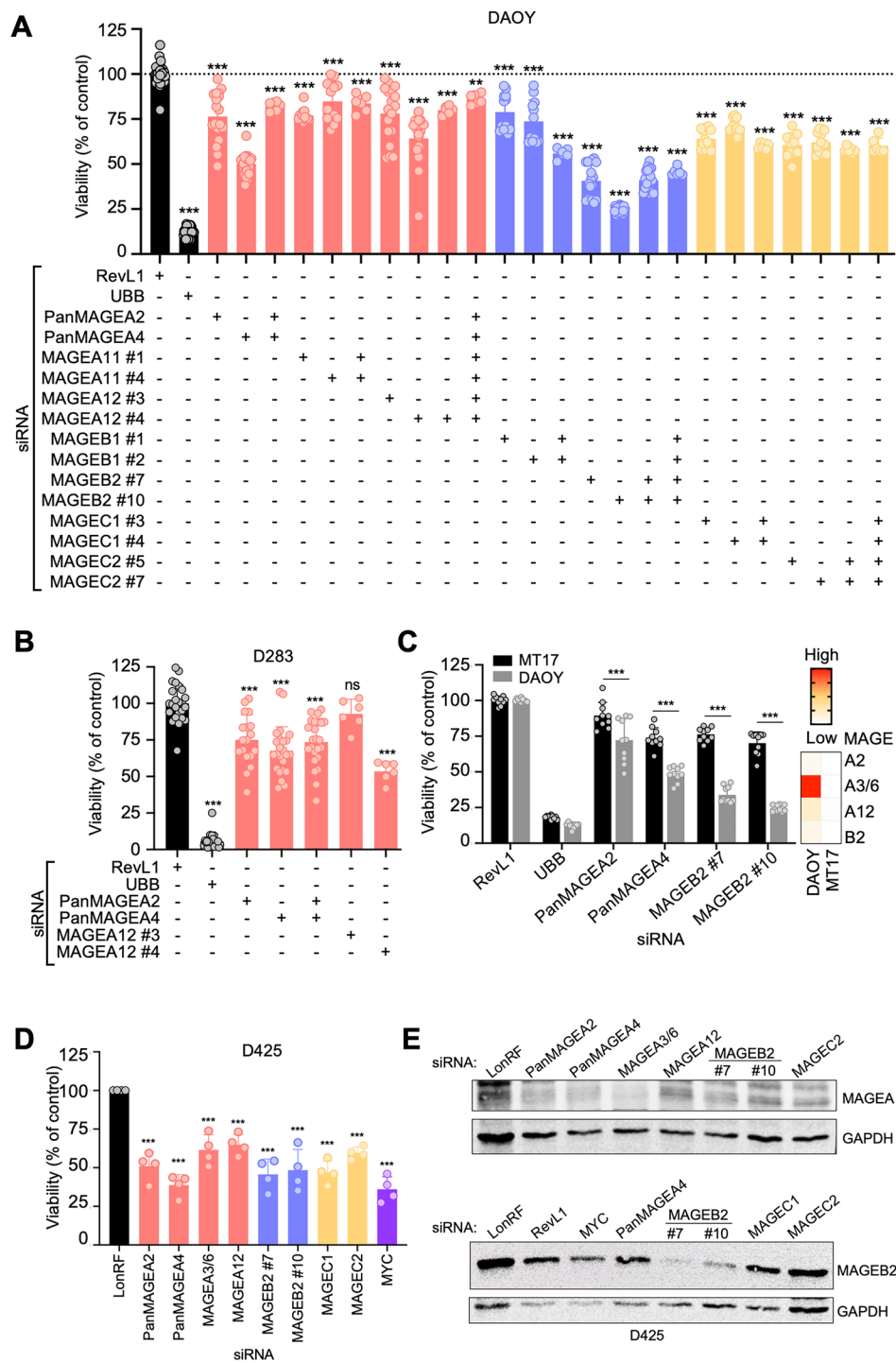


Fig. 4 (See legend on previous page.)

differently than the current consensus [55]. Consistent with previous analyses of individual *MAGE-A* and *-C* family members [23, 27, 43, 50], we found that at least one Type I *MAGE* is expressed in more than half of pediatric MBs (Fig. 1). *MAGE* expression was particularly evident

in group 3 MBs, which is considered the most aggressive MB subgroup, with a 5-year overall survival of less than 60% [29]. *MAGEA1*, *-A2*, *-A3/6*, *-A12*, *-B2*, and *-C2* are specifically enriched in Group 3 tumors. Moreover, these *MAGE* genes exhibit the highest expression levels among

all Type I *MAGE* genes in medulloblastoma samples (Figs. 1B–D, 2B, and 2C). In contrast, other *MAGE* genes (i.e., *MAGEA8*, *-A10*, *-B10*, *-B17*, and *-C3*) show broader expression across all samples, while *MAGEA11* and *-C1* tend to be more associated with the WNT subgroup. Although group 3 MBs exhibit some notable genomic features, such as specific aneuploidies and amplification of *MYC*, *MYCN*, or *OTX2*, the unresolved molecular heterogeneity of these tumors contributes to the low therapeutic success reported in patients [18, 29, 39].

We discovered that more than 60% of group 3 MBs express at least one, but often several, *MAGE* genes (Figs. 1, 2, and S1–S3). Different *MAGE* genes are often expressed in distinct subsets of cells (Figs. S2 and S3, Tables S4 and S5), suggesting they contribute to the intra- and inter-tumor heterogeneity of MBs. However, further studies are needed to identify the epigenetic and transcriptional mechanisms responsible for activating aberrant *MAGE* expression in MBs. The co-expression of multiple Type I *MAGEs* in neoplastic cells may impart oncogenic functions, such as increased survival and proliferation, due to synergistic molecular effects or these proteins acting together [30]. Accordingly, *MAGE* expression in various cancers is associated with chemoresistance and a worse prognosis [10, 12, 13, 37, 38, 53]. In the testis, subsets of *MAGE* genes are expressed in distinct populations of male germ cells during differentiation, starting from spermatogonial stem cells through haploid spermatids, suggesting autocrine and paracrine functions [15]. Importantly, we previously reported that *MAGE* genes protect the germline against diverse stressors (e.g., nutritional stress, chemotherapy, and heat), indicating that their protective functions may have evolved to protect male fertility but are hijacked by cancer cells to increase their growth and therapy resistance [15, 31]. Therefore, *MAGE* expression signature may contribute to better stratification of and therapy selection for group 3 patients.

Targeting these aberrantly expressed *MAGEs* or the pathways they regulate may represent potential therapeutic opportunities, including immunotherapy. Their restricted tissue expression [15] may lead to a lower probability of side effects and toxicity, critically important

in the pediatric population that is still undergoing brain development [29]. The decreased viability, proliferation, and colony formation we observed upon depletion of Type I *MAGEs* (Figs. 3, 4, and 5) suggests that these genes play a role in the proliferation and viability of MB cells and supports targeting *MAGEs* as a potential mode of MB cancer therapy. However, further investigation into the molecular functions of these *MAGEs* in MBs is needed. The expression of *MAGEs* in group 3 is especially attractive, as current therapeutic options are limited and have a high risk of neurotoxicity [8, 36, 55]. Targeting multiple *MAGEs* concurrently may further allow for a synergistic effect of therapy while reducing the side effects.

Additionally, we found that the *MAGE* expression profile in PDOX models mirrored the tumors (Fig. 2). Given that the group 3 cell of origin is human-specific and not found in mice [51], these PDOX models represent an important experimental model for studying *MAGEs* in group 3 MBs. In contrast to adult cancers, which are frequently attributable to genomic alterations due to repeated environmental exposures, childhood malignancies are more often the consequence of failed developmental processes [24]. We previously found that several Type I *MAGEs* are expressed more broadly during embryonic development, particularly in the brain, indicating they may be involved in developmental processes and, when derailed, contribute to oncogenic transformation [15]. Prototypic group 3 MBs are predominantly comprised of undifferentiated progenitor-like cells with high *MYC* activity [21], suggesting that the undifferentiated transcriptional program of these cells may be connected to their aberrant expression of multiple *MAGEs*. However, the expression patterns of *MYC* and *MAGEs* (Figs. 1C, 1D, 2C, and 3A), along with the viability data from the D341 *MYC*-amplified medulloblastoma cell line (Figs. 4D, 4E, and S5B–D), suggest that *MAGE* expression may be independent of *MYC* expression. Furthermore, the undetectable expression of *Mages* in tumors from murine genetic MB models further corroborates the species-specificity of this subtype and calls for enhanced development of

(See figure on next page.)

Fig. 5 Knockdown of *MAGEs* decreases colony formation and cell proliferation and increases apoptosis. **A** DAOY cells were transfected with the indicated siRNA and BrdU immunofluorescence assay was performed 48 h later. Representative images of stained cells are shown. **B** Graph shows the percentage of BrdU-positive cells, relative to the siRevL1 control, determined by counting at least 100 cells for each condition ($n=2$). **C** Transfected DAOY cells were plated for a soft agar assay, and colonies were imaged after 4 weeks. Representative images for each siRNA are shown. **D** The number of colonies for each condition was normalized to the siLonRF control to calculate the percentage ($n=3$). **E** DAOY cells were transfected with indicated siRNA and collected 48 h after transfection for western blotting. siMAGEB2s and, to a lesser extent, siPanMAGEA4 increased cleavage of PARP, indicative of increased apoptosis. Significance was assessed with one-way ANOVA followed by Dunnett's multiple comparisons test for samples compared to the siRevL1 or siLonRF control [$P \leq 0.05$ (*), $P \leq 0.01$ (**), $P > 0.05$ (non-significant, ns)]

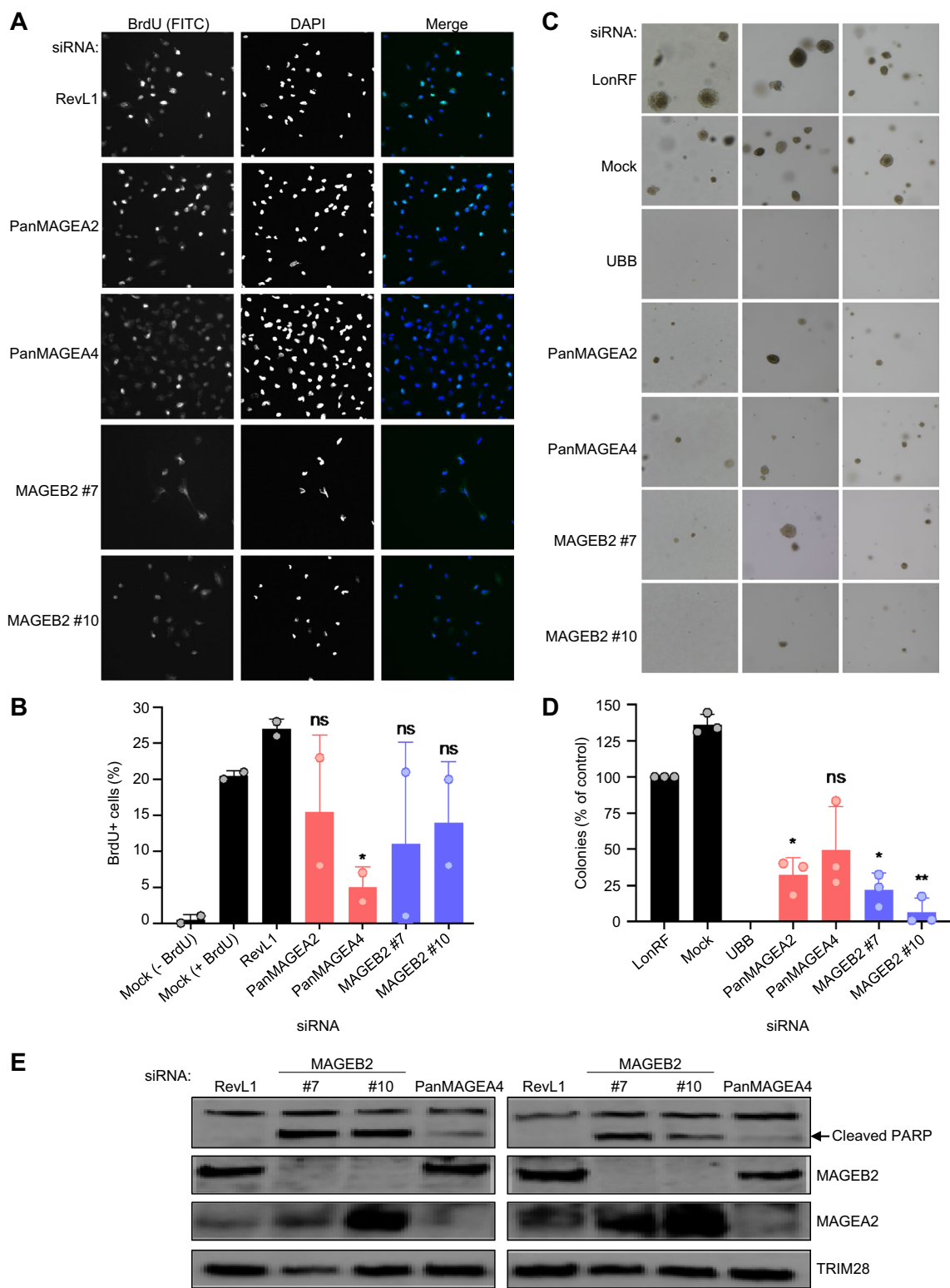


Fig. 5 (See legend on previous page.)

patient-derived models, including PDOXs and organoids, to substitute for laboratory rodents.

In conclusion, we report that Type I *MAGEs* are expressed in more than half of pediatric MBs, particularly in group 3 tumors. Further investigation into their tumor-intrinsic functions and impact on the immune microenvironment is needed, as *MAGEs* represent an exciting opportunity to address the biggest unmet needs for group 3 MB patients: rigorous preclinical biomarkers and therapeutic targets. The depletion of *MAGEs* led to decreased viability, proliferation, and colony formation in MB cell lines, suggesting that *MAGE*-targeted therapy could enhance chemosensitivity in *MAGE*-positive MBs. Further preclinical research is needed to better understand potential therapeutic vulnerabilities of *MAGE*-positive group 3 MBs and how these can be preclinically tested using more accurate models.

Supplementary Information

The online version contains supplementary material available at <https://doi.org/10.1186/s40478-025-02055-3>.

Additional file1
Additional file2
Additional file3
Additional file4
Additional file5
Additional file6
Additional file7
Additional file8

Acknowledgements

We thank members of the Fon Tacer and Potts laboratories for their advice and critical discussions. The graphical abstract and Figures 1A and 3B were created with BioRender (BioRender.com).

Author contributions

RRJC, PRP, and KFT conceived and designed the research. RRJC, RRF, AKL, MCHS, ST, TB, JSSG, and BB conducted experiments and analyzed data. RRJC, RRF, MCHS, TB, ST, and KFT wrote the manuscript. MFR, STP, JPC, and SMP-M developed reagents, and DR provided resources for this study. All authors have approved the final manuscript.

Funding

Funding for this work was supported by National Institutes of Health National Cancer Institute (T32CA136515 to RRJC, CA096832 and CA21765 to MFR); American Cancer Society Research Scholar Award (181691010 to PRP); and Cancer Prevention and Research Institute of Texas (R1117 to PRP, RR200059 to KFT); the Texas Tech University start-up and the Texas Center for Comparative Cancer Research (TC3R) (KFT); Foundation for Prader–Willi Syndrome Research Grants (22-0321 and 23-0447 to KFT); Fulbright fellowship (to BB); Slovenian Research and Innovation Agency (program P1-0245, projects J3-4504, BI-US/22-24-007 to BB and BI-US/24-26-022 to KFT and BB); Horizon Europe CutCancer project (101079113 to BB); John Lawrence and Patsy Louise Goforth Distinguished Chair in Pathology endowment (to DR); and the American Lebanese Syrian Associated Charities of St Jude Children's Research Hospital.

Availability of data and materials

Data and material generated in this work are available upon request. Publicly available data accession numbers are reported above in the Materials and Method section.

Declarations

Competing interests

None declared.

Consent for publication

Authors all agree with publication.

Author details

¹Department of Pathology, University of Texas Southwestern Medical Center, Dallas, TX 75390, USA. ²School of Veterinary Medicine, Texas Tech University, 7671 Evans Dr., Amarillo, TX 79106, USA. ³Texas Center for Comparative Cancer Research (TC3R), Amarillo, TX 79106, USA. ⁴Graduate School of Biomedical Sciences, St. Jude Children's Research Hospital, Memphis, TN 38105, USA. ⁵Department of Cell and Molecular Biology, St. Jude Children's Research Hospital, Memphis, TN 38105, USA. ⁶Department of Genetic Toxicology and Cancer Biology, National Institute of Biology, 121 Večna Pot, 1000 Ljubljana, Slovenia. ⁷Department of Physiology, University of Texas Southwestern Medical Center, Dallas, TX 75390, USA. ⁸Center for Advanced Genome Engineering, St. Jude Children's Research Hospital, Memphis, TN 38105, USA. ⁹Department of Tumor Cell Biology, St. Jude Children's Research Hospital, Memphis, TN 38105, USA. ¹⁰Department of Pathology, Children's Medical Center, Dallas, TX 75235, USA. ¹¹Department of Pathology, St. Jude Children's Research Hospital, Memphis, TN 38105, USA. ¹²Induced Proximity Platform, Amgen Research, Thousand Oaks, CA 91320, USA.

Received: 18 July 2024 Accepted: 5 June 2025

Published online: 28 July 2025

References

- Abbott RC, Cross RS, Jenkins MR (2020) Finding the keys to the CAR: identifying novel target antigens for T cell redirection immunotherapies. *Int J Mol Sci* 21:1. <https://doi.org/10.3390/ijms21020515>
- Alexandrov LB, Nik-Zainal S, Wedge DC, Aparicio SA, Behjati S, Biankin AV, Bignell GR, Bolli N, Borg A, Borresen-Dale AL et al (2013) Signatures of mutational processes in human cancer. *Nature* 500:415–421. <https://doi.org/10.1038/nature12477>
- Alsalloum A, Shevchenko JA, Sennikov S (2023) The melanoma-associated antigen family a (MAGE-A): a promising target for cancer immunotherapy? *Cancers (Basel)* 15:5. <https://doi.org/10.3390/cancers15061779>
- Barretina J, Caponigro G, Stransky N, Venkatesan K, Margolin AA, Kim S, Wilson CJ, Lehar J, Kryukov GV, Sonkin D et al (2012) The cancer cell line encyclopedia enables predictive modelling of anticancer drug sensitivity. *Nature* 483:603–607. <https://doi.org/10.1038/nature11003>
- Bowman RL, Wang Q, Carro A, Verhaak RG, Squatrito M (2017) Gliovis data portal for visualization and analysis of brain tumor expression datasets. *Neuro Oncol* 19:139–141. <https://doi.org/10.1093/neuonc/now247>
- Casciati A, Tanori M, Manczak R, Saada S, Tanno B, Giardullo P, Porcu E, Rampazzo E, Persano L, Viola G et al (2020) Human medulloblastoma cell lines: investigating on cancer stem cell-like phenotype. *Cancers (Basel)*. <https://doi.org/10.3390/cancers12010226>
- Casey DL, Cheung NV (2020) Immunotherapy of pediatric solid tumors: treatments at a crossroads, with an emphasis on antibodies. *Cancer Immunol Res* 8:161–166. <https://doi.org/10.1158/2326-6066.CIR-19-0692>
- Cavalli FMG, Remke M, Rampasek L, Peacock J, Shih DJH, Luu B, Garzia L, Torchia J, Nor C, Morrissey AS et al (2017) Intertumoral heterogeneity within medulloblastoma subgroups. *Cancer Cell* 31(737–754):e736. <https://doi.org/10.1016/j.ccell.2017.05.005>
- Chen X, Wang L, Liu J, Huang L, Yang L, Gao Q, Shi X, Li J, Li F, Zhang Z et al (2017) Expression and prognostic relevance of MAGE-A3 and MAGE-C2 in non-small cell lung cancer. *Oncol Lett* 13:1609–1618. <https://doi.org/10.3892/ol.2017.5665>

10. Cuffel C, Rivals JP, Zaugg Y, Salvi S, Seelentag W, Speiser DE, Lienard D, Monnier P, Romero P, Bron L et al (2011) Pattern and clinical significance of cancer-testis gene expression in head and neck squamous cell carcinoma. *Int J Cancer* 128:2625–2634. <https://doi.org/10.1002/ijc.25607>
11. Doyle JM, Gao J, Wang J, Yang M, Potts PR (2010) MAGE-RING protein complexes comprise a family of E3 ubiquitin ligases. *Mol Cell* 39:963–974. <https://doi.org/10.1016/j.molcel.2010.08.029>
12. Duan Z, Duan Y, Lamendola DE, Yusuf RZ, Naeem R, Penson RT, Seiden MV (2003) Overexpression of MAGE/GAGE genes in paclitaxel/doxorubicin-resistant human cancer cell lines. *Clin Cancer Res* 9:2778–2785
13. Faiena I, Astrow SH, Elashoff DA, Jain R, Bot A, Chamie K, Beldegrun AS, Pantuck AJ, Drakaki A (2019) Melanoma-associated antigen-A and programmed death-ligand 1 expression are associated with advanced urothelial carcinoma. *Cancer Immunol Immunother* 68:743–751. <https://doi.org/10.1007/s00262-019-02316-w>
14. Florke Gee RR, Chen H, Lee AK, Daly CA, Wilander BA, Fon Tacer K, Potts PR (2020) Emerging roles of the MAGE protein family in stress response pathways. *J Biol Chem* 295:16121–16155. <https://doi.org/10.1074/jbc.REV120.008029>
15. Fon Tacer K, Montoya MC, Oatley MJ, Lord T, Oatley JM, Klein J, Ravichandran R, Tillman H, Kim M, Connelly JP et al (2019) MAGE cancer-testis antigens protect the mammalian germline under environmental stress. *Sci Adv* 5:eav4832. <https://doi.org/10.1126/sciadv.aav4832>
16. Friedman HS, Burger PC, Bigner SH, Trojanowski JQ, Wikstrand CJ, Halperin EC, Bigner DD (1985) Establishment and characterization of the human medulloblastoma cell line and transplantable xenograft D283 Med. *J Neuropathol Exp Neurol* 44:592–605. <https://doi.org/10.1097/00005072-198511000-00005>
17. Gibbs ZA, Whitehurst AW (2018) Emerging contributions of cancer/testis antigens to neoplastic behaviors. *Trends Cancer* 4:701–712. <https://doi.org/10.1016/j.trecan.2018.08.005>
18. Goschzik T, Schwalbe EC, Hicks D, Smith A, Zur Muehlen A, Figarella-Branger D, Doz F, Rutkowski S, Lannering B, Pietsch T et al (2018) Prognostic effect of whole chromosomal aberration signatures in standard-risk, non-WNT/non-SHH medulloblastoma: a retrospective, molecular analysis of the HIT-SIOP PNET 4 trial. *Lancet Oncol* 19:1602–1616. [https://doi.org/10.1016/S1470-2045\(18\)30532-1](https://doi.org/10.1016/S1470-2045(18)30532-1)
19. Haldipur P, Aldinger KA, Bernardo S, Deng M, Timms AE, Overman LM, Winter C, Lisgo SN, Razavi F, Silvestri E et al (2019) Spatiotemporal expansion of primary progenitor zones in the developing human cerebellum. *Science* 366:454–460. <https://doi.org/10.1126/science.aax7526>
20. Haydar D, Ibanez-Vega J, Krenciute G (2021) T-cell immunotherapy for pediatric high-grade gliomas: new insights to overcoming therapeutic challenges. *Front Oncol* 11:718030. <https://doi.org/10.3389/fonc.2021.718030>
21. Hovestadt V, Smith KS, Bihannic L, Filbin MG, Shaw ML, Baumgartner A, DeWitt JC, Groves A, Mayr L, Weisman HR et al (2019) Resolving medulloblastoma cellular architecture by single-cell genomics. *Nature* 572:74–79. <https://doi.org/10.1038/s41586-019-1434-6>
22. Ivanov DP, Coyle B, Walker DA, Grabowska AM (2016) In vitro models of medulloblastoma: choosing the right tool for the job. *J Biotechnol* 236:10–25. <https://doi.org/10.1016/j.jbiotec.2016.07.028>
23. Jacobs JF, Grauer OM, Brasseur F, Hoogerbrugge PM, Wesseling P, Gidding CE, van de Rakt MW, Figdor CG, Coulie PG, de Vries IJ et al (2008) Selective cancer-germline gene expression in pediatric brain tumors. *J Neurooncol* 88:273–280. <https://doi.org/10.1007/s11060-008-9577-6>
24. Jones DTW, Banito A, Grunewald TGP, Haber M, Jager N, Kool M, Milde T, Molenaar JJ, Nabbi A, Pugh TJ et al (2019) Molecular characteristics and therapeutic vulnerabilities across paediatric solid tumours. *Nat Rev Cancer* 19:420–438. <https://doi.org/10.1038/s41568-019-0169-x>
25. Joung J, Konermann S, Gootenberg JS, Abudayyeh OO, Platt RJ, Brigham MD, Sanjana NE, Zhang F (2017) Genome-scale CRISPR-Cas9 knockout and transcriptional activation screening. *Nat Protoc* 12:828–863. <https://doi.org/10.1038/nprot.2017.016>
26. Juraschka K, Taylor MD (2019) Medulloblastoma in the age of molecular subgroups: a review. *J Neurosurg Pediatr* 24:353–363. <https://doi.org/10.3171/2019.5.PEDS18381>
27. Kasuga C, Nakahara Y, Ueda S, Hawkins C, Taylor MD, Smith CA, Rutka JT (2008) Expression of MAGE and GAGE genes in medulloblastoma and modulation of resistance to chemotherapy. Laboratory investigation. *J Neurosurg Pediatr* 1:305–313. <https://doi.org/10.3171/PED/2008/1/4/305>
28. Kool M, Korshunov A, Remke M, Jones DT, Schlanstein M, Northcott PA, Cho YJ, Koster J, Schouten-van Meeteren A, van Vuurden D et al (2012) Molecular subgroups of medulloblastoma: an international meta-analysis of transcriptome, genetic aberrations, and clinical data of WNT, SHH, Group 3, and Group 4 medulloblastomas. *Acta Neuropathol* 123:473–484. <https://doi.org/10.1007/s00401-012-0958-8>
29. Kumar R, Liu APY, Northcott PA (2020) Medulloblastoma genomics in the modern molecular era. *Brain Pathol* 30:679–690. <https://doi.org/10.1111/bpa.12804>
30. Laiseca JE, Ladelfa MF, Cotignola J, Pêche LY, Pascucci FA, Castano BA, Galigniana MD, Schneider C, Monte M (2017) Functional interaction between co-expressed MAGE-A proteins. *PLoS ONE* 12:e0178370. <https://doi.org/10.1371/journal.pone.0178370>
31. Lee AK, Klein J, Fon Tacer K, Lord T, Oatley MJ, Oatley JM, Porter SN, Pruett-Miller SM, Tikhonova EB, Karamyshev AL et al (2020) Translational repression of G3BP in cancer and germ cells suppresses stress granules and enhances stress tolerance. *Mol Cell* 79(645–659):e649. <https://doi.org/10.1016/j.molcel.2020.06.037>
32. Lee AK, Potts PR (2017) A comprehensive guide to the MAGE family of ubiquitin ligases. *J Mol Biol* 429:1114–1142. <https://doi.org/10.1016/j.jmb.2017.03.005>
33. Li W, Koster J, Xu H, Chen CH, Xiao T, Liu JS, Brown M, Liu XS (2015) Quality control, modeling, and visualization of CRISPR screens with MAGECK-VISPR. *Genome Biol* 16:281. <https://doi.org/10.1186/s13059-015-0843-6>
34. Liu KW, Pajitler KW, Worst BC, Pfister SM, Wechsler-Reya RJ (2017) Molecular mechanisms and therapeutic targets in pediatric brain tumors. *Sci Signal*. <https://doi.org/10.1126/scisignal.aaf7593>
35. Louis DN, Perry A, Wesseling P, Brat DJ, Cree IA, Figarella-Branger D, Hawkins C, Ng HK, Pfister SM, Reifenberger G et al (2021) The 2021 WHO classification of tumors of the central nervous system: a summary. *Neuro Oncol* 23:1231–1251. <https://doi.org/10.1093/neuonc/noab106>
36. Luo Z, Xin D, Liao Y, Berry K, Ogurek S, Zhang F, Zhang L, Zhao C, Rao R, Dong X et al (2023) Loss of phosphatase CTDNEP1 potentiates aggressive medulloblastoma by triggering MYC amplification and genomic instability. *Nat Commun* 14:762. <https://doi.org/10.1038/s41467-023-36400-8>
37. Monte M, Simonatto M, Pêche LY, Bublik DR, Gobessi S, Pierotti MA, Rodolfo M, Schneider C (2006) MAGE-A tumor antigens target p53 transactivation function through histone deacetylase recruitment and confer resistance to chemotherapeutic agents. *Proc Natl Acad Sci U S A* 103:11160–11165. <https://doi.org/10.1073/pnas.0510834103>
38. Napolitano C, Bellati F, Tarquini E, Tomao F, Taurino F, Spagnoli G, Rugghetti A, Muzii L, Nuti M, Benedetti Panici P (2008) MAGE-A and NY-ESO-1 expression in cervical cancer: prognostic factors and effects of chemotherapy. *Am J Obstet Gynecol* 198(99):e91–97. <https://doi.org/10.1016/j.ajog.2007.05.019>
39. Northcott PA, Buchhalter I, Morrissy AS, Hovestadt V, Weischenfeldt J, Ehrenberger T, Grobner S, Segura-Wang M, Zichner T, Rudneva VA et al (2017) The whole-genome landscape of medulloblastoma subtypes. *Nature* 547:311–317. <https://doi.org/10.1038/nature22973>
40. Northcott PA, Jones DT, Kool M, Robinson GW, Gilbertson RJ, Cho YJ, Pomeroy SL, Korshunov A, Lichter P, Taylor MD et al (2012) Medulloblastomas: the end of the beginning. *Nat Rev Cancer* 12:818–834. <https://doi.org/10.1038/nrc3410>
41. Northcott PA, Korshunov A, Witt H, Hielscher T, Eberhart CG, Mack S, Bouffet E, Clifford SC, Hawkins CE, French P et al (2011) Medulloblastoma comprises four distinct molecular variants. *J Clin Oncol* 29:1408–1414. <https://doi.org/10.1200/JCO.2009.27.4324>
42. Northcott PA, Robinson GW, Kratz CP, Mabbott DJ, Pomeroy SL, Clifford SC, Rutkowski S, Ellison DW, Malkin D, Taylor MD et al (2019) Medulloblastoma. *Nat Rev Dis Primers* 5:11. <https://doi.org/10.1038/s41572-019-0063-6>
43. Oba-Shinjo SM, Caballero OL, Jungbluth AA, Rosemberg S, Old LJ, Simpson AJ, Marie SK (2008) Cancer-testis (CT) antigen expression in medulloblastoma. *Cancer Immun* 8:7
44. Phoenix TN, Patmore DM, Boop S, Boulos N, Jacus MO, Patel YT, Roussel MF, Finkelstein D, Goumnerova L, Perreault S et al (2016) Medulloblastoma genotype dictates blood brain barrier phenotype. *Cancer Cell* 29:508–522. <https://doi.org/10.1016/j.ccell.2016.03.002>
45. Pineda CT, Ramanathan S, Fon Tacer K, Weon JL, Potts MB, Ou YH, White MA, Potts PR (2015) Degradation of AMPK by a cancer-specific ubiquitin ligase. *Cell* 160:715–728. <https://doi.org/10.1016/j.cell.2015.01.034>

46. Potts PR, Porteus MH, Yu H (2006) Human SMC5/6 complex promotes sister chromatid homologous recombination by recruiting the SMC1/3 cohesin complex to double-strand breaks. *EMBO J* 25:3377–3388. <https://doi.org/10.1038/sj.emboj.7601218>
47. Riemondy KA, Venkataraman S, Willard N, Nellan A, Sanford B, Griesinger AM, Amani V, Mitra S, Hankinson TC, Handler MH et al (2022) Neoplastic and immune single-cell transcriptomics define subgroup-specific intra-tumoral heterogeneity of childhood medulloblastoma. *Neuro Oncol* 24:273–286. <https://doi.org/10.1093/neuonc/noab135>
48. Roussel MF, Hatten ME (2011) Cerebellum development and medulloblastoma. *Curr Top Dev Biol* 94:235–282. <https://doi.org/10.1016/B978-0-12-380916-2.00008-5>
49. Roussel MF, Stripay JL (2020) Modeling pediatric medulloblastoma. *Brain Pathol* 30:703–712. <https://doi.org/10.1111/bpa.12803>
50. Scarcella DL, Chow CW, Gonzales MF, Economou C, Brasseur F, Ashley DM (1999) Expression of MAGE and GAGE in high-grade brain tumors: a potential target for specific immunotherapy and diagnostic markers. *Clin Cancer Res* 5:335–341
51. Smith KS, Bihannic L, Gudenas BL, Haldipur P, Tao R, Gao Q, Li Y, Aldinger KA, Iskushnykh IY, Chizhikov VV et al (2022) Unified rhombic lip origins of group 3 and group 4 medulloblastoma. *Nature* 609:1012–1020. <https://doi.org/10.1038/s41586-022-05208-9>
52. Smith KS, Xu K, Mercer KS, Boop F, Klimo P, DeCupere M, Grenet J, Robinson S, Dunphy P, Baker SJ et al (2020) Patient-derived orthotopic xenografts of pediatric brain tumors: a St. Jude resource. *Acta Neuropathol* 140:209–225. <https://doi.org/10.1007/s00401-020-02171-5>
53. Suzuki T, Yoshida K, Wada Y, Hamai Y, Sentani K, Oue N, Yasui W (2007) Melanoma-associated antigen-A1 expression predicts resistance to docetaxel and paclitaxel in advanced and recurrent gastric cancer. *Oncol Rep* 18:329–336
54. Tacer KF, Potts PR (2017) Cellular and disease functions of the Prader-Willi Syndrome gene MAGEL2. *Biochem J* 474:2177–2190. <https://doi.org/10.1042/BCJ20160616>
55. Taylor MD, Northcott PA, Korshunov A, Remke M, Cho YJ, Clifford SC, Eberhart CG, Parsons DW, Rutkowski S, Gajjar A et al (2012) Molecular subgroups of medulloblastoma: the current consensus. *Acta Neuropathol* 123:465–472. <https://doi.org/10.1007/s00401-011-0922-z>
56. Thomas A, Noel G (2019) Medulloblastoma: optimizing care with a multi-disciplinary approach. *J Multidiscip Healthc* 12:335–347. <https://doi.org/10.2147/JMDH.S167808>
57. Vladoiu MC, El-Hamamy I, Donovan LK, Farooq H, Holgado BL, Sundaravadanam Y, Ramaswamy V, Hendrikse LD, Kumar S, Mack SC et al (2019) Childhood cerebellar tumours mirror conserved fetal transcriptional programs. *Nature* 572:67–73. <https://doi.org/10.1038/s41586-019-1158-7>
58. Weon JL, Potts PR (2015) The MAGE protein family and cancer. *Curr Opin Cell Biol* 37:1–8. <https://doi.org/10.1016/j.ceb.2015.08.002>
59. Williamson D, Schwalbe EC, Hicks D, Aldinger KA, Lindsey JC, Crosier S, Richardson S, Goddard J, Hill RM, Castle J et al (2022) Medulloblastoma group 3 and 4 tumors comprise a clinically and biologically significant expression continuum reflecting human cerebellar development. *Cell Rep* 40:111162. <https://doi.org/10.1016/j.celrep.2022.111162>
60. Xie C, Subhash VV, Datta A, Liem N, Tan SH, Yeo MS, Tan WL, Koh V, Yan FL, Wong FY et al (2016) Melanoma associated antigen (MAGE)-A3 promotes cell proliferation and chemotherapeutic drug resistance in gastric cancer. *Cell Oncol (Dordr)* 39:175–186. <https://doi.org/10.1007/s13402-015-0261-5>
61. Xie N, Shen G, Gao W, Huang Z, Huang C, Fu L (2023) Neoantigens: promising targets for cancer therapy. *Signal Transduct Target Ther* 8:9. <https://doi.org/10.1038/s41392-022-01270-x>
62. Yang SW, Li L, Connelly JP, Porter SN, Kodali K, Gan H, Park JM, Tacer KF, Tillman H, Peng J et al (2020) A cancer-specific ubiquitin ligase drives mrna alternative polyadenylation by ubiquitinating the mRNA 3' end processing complex. *Mol Cell* 77(1206–1221):e1207. <https://doi.org/10.1016/j.molcel.2019.12.022>

Publisher's Note

Springer Nature remains neutral with regard to jurisdictional claims in published maps and institutional affiliations.